JET-P(95)34

A Vacuum Ultra-violet Spectrometer (Double SPRED) for the Observation of the JET Divertor Plasma

R C Wolf[1], K D Lawson[2], I Coffey[3], R Giannella, C J Hancock, N C Hawkes[2], L D Horton, G Janeschitz[4], H Jemmeson, A C Maas, C F Maggi, M Di Maio.

JET Joint Undertaking, Abingdon, Oxfordshire, OX14 3EA, UK.
[1]Present address: Max-Planck-Institut für Plasmaphysik, Bereich Berlin, Mohrenstr. 40/41, D-10117 Berlin, Germany.
[2] UKAEA Government Division, Fusion, Culham, Abingdon, OX14 3DB, UK. (UKAEA/EURATOM Fusion Association).
[3] Dept. Pure & Applied Physics, Queens University, Belfast, BT7 1NN, N. Ireland.
[4] Present address: ITER, Garching, Germany.

Preprint of a paper to be submitted for publication in Review of Scientific Instruments

September 1995

Abstract

The SPRED spectrometer is a VUV survey instrument that has been successfully employed on a number of plasma machines. Its use of a holographic grating results in a flat focal field, enabling the best spectral resolution to be achieved over the whole extent of the detector. A double SPRED spectrometer having two fixed gratings and two independently controlled detectors has been installed on the JET machine for the observation of the divertor plasma. An additional improvement over previous SPRED designs is the extended wavelength coverage of the detectors. The experimental setup, including the spectrometer design, the VUV detectors, the alignment and control systems are described. The commissioning of the spectrometer on JET has allowed the performance of the instrument to be assessed, in particular its wavelength calibration, spectral resolution and the effect of the integral shielding to nuclear radiation-induced noise. First results include a comparison with the spectral emission from the bulk plasma of the JET tokamak, observed with a single SPRED instrument, which emphasizes that the dominant emission from the divertor originates from low ionization stages of low Z-impurities such as carbon. Evidence has been found for the localization of the line emission from within the divertor chamber and some features of the divertor VUV radiation during high performance plasmas are described. Future applications are also discussed.

1. Introduction

The need to study the impurity behavior in high temperature plasmas led to the development of the SPRED VUV survey spectrometer [Fonck 82]. It enables time-resolved, impurity spectra to be observed over a wide range of the VUV wavelength region with a moderate spectral resolution. The use of a holographic diffraction grating produces a flat focal field, thus avoiding a loss of spectral resolution towards the edges of the detector. Depending on the grating used, wavelengths from 100 to 1700 Å are covered. Spectrometers of the SPRED design have been operated successfully on several fusion devices [Stratton 86, Wood 88, Janeschitz 90, Carraro 89, Carraro 93, Brzozowski 91, Zastrow 93].

In previous plasma operations, a single SPRED spectrometer with three interchangeable gratings (290 g/mm, 450 g/mm and 2105 g/mm) was employed on JET to view the bulk plasma with a near horizontal line of sight at the tokamak midplane [Hawkes 93]. With the upgrade of the JET machine, which included the installation of a single-null pumped divertor inside the JET vessel [Bertolini 95], an additional double SPRED spectrometer has been installed on top of the vessel to investigate the divertor plasma (fig. 1). The JET double SPRED instrument combines two fixed gratings (450 g/mm and 2105 g/mm) in a single vacuum chamber, allowing two spectra with different spectral ranges and resolutions to be recorded simultaneously. In addition the detectors have been modified to give each one an extended wavelength coverage.

So as to gain understanding of the impurity transport within the divertor region, the double SPRED spectrometer enables the simultaneous measurement of deuterium and impurity spectral lines. For example, the extended wavelength range of the combined detector assembly allows line emission from all ionization stages of carbon to be observed in addition to deuterium, the former being the dominant low Z impurity in the present JET divertor. Most present day fusion machines use low Z first wall materials such as carbon or beryllium in order to reduce the effect of sputtered wall materials on the radiative power loss. Such low Z impurities radiate primarily from the plasma edge and from the divertor region of a tokamak such as JET. As an example, a typical 2-D spatial distribution of the CIV density is shown in fig. 2, this being a result of a simulation of the JET divertor plasma using the DIVIMP impurity Monte Carlo transport code [Stangeby 92]. It can be seen that the highest CIV ion density is located near to the divertor target, indicating that for the low ionization stages of these low Z impurities the line radiation is localized within the divertor chamber. This implies that, despite a line integration along a vertical viewing line, the signals are dominated by the divertor emission.

The paper is structured as follows; first, the design of the double SPRED spectrometer is discussed. The experimental setup, which has to fulfill the requirements of a large fusion device such as JET, is presented. These requirements include radiation shielding and a special alignment system. The spectrometer and detector assembly are

discussed emphasizing the improvements made over previous SPRED designs. A control system is introduced, which is based on a novel fiber optic field bus. The performance of the spectrometer and detectors has been investigated, including the gain behavior, wavelength calibration and spectral dispersion. Attention is drawn to the spectral resolution, in particular with regard to the extended spectral range of each detector. The effect of the shielding is estimated and, finally, some first experimental results are presented, showing the quality of the data obtained both with regard to its spectral and temporal resolution.

2. Double-SPRED Spectrometer

2.1. Experimental Setup

An overview of the double SPRED spectrometer showing its position on the machine and its view of the JET divertor is given in fig. 1. The spectrometer is mounted on a frame. This is attached to a motor drive, which allows the spectrometer assembly to be moved around the pivot point by 12° and, hence, the total divertor region to be scanned radially [Walker 94]. The spectrometer components, which are shown in fig. 3, are mounted within a forged stainless steel block, weighing 350 kg, the main function of which is to shield the detectors from neutrons and γ-rays produced during high performance discharges. To minimize the total mass of the spectrometer the shielding has been placed as close as possible to the detectors. The effect of this shielding is discussed in section 3.4. A central bore through the SPRED vacuum chamber provides a viewing line for an additional spectrometer or other light collection system. Initial tests were carried out using a high resolution multi-channel soft x-ray spectrometer [Schwob 87]. This was subsequently replaced by an optical fibre connected to a visible spectrometer having an absolute sensitivity calibration, which will allow an 'in situ' sensitivity calibration of the double SPRED instrument using the branching ratio technique.

2.2. Alignment system

A chamber containing several mirrors on a rotary table (fig. 3) has been designed for the alignment of the spectrometer assembly. This chamber is installed between the spectrometer and the torus interface. The table can be rotated while the instrument is pumped, thus allowing the alignment to be performed under vacuum. Light from a He-Ne laser can be reflected in the following directions: (A) through the spectrometer slits onto the center of the SPRED gratings, (B) through the central bore of the SPRED vacuum chamber and (C) into the torus. (A) allows the alignment of the slits and baffles relative to the gratings to be checked. In the case of (B) and (C) the laser beam represents the axis of symmetry of the viewing lines and hence can be utilized to align the SPRED spectrometers and any additional instrument relative to the torus.

In addition, the mirror chamber is equipped with a set of spherical mirrors, which image light, for instance, from a deuterium spectral lamp onto the spectrometer slits. The spectra obtained can be used for such purposes as wavelength calibration, detector focusing or the verification of the detector sensitivity.

2.3. Spectrometer arrangement

The JET double SPRED spectrometer (McPherson, model 251 M2) consists of two independent SPRED spectrometers [Fonck 82] with fixed gratings, mounted back to back, in the same vacuum chamber (fig. 3). The lines of sight of the spectrometers, inclined at 0.6° to one another, meet on the divertor target plates. The two toroidal gratings (Jobin-Yvon Optical Systems) have groove densities of 450 g/mm [Fonck 82] and 2105 g/mm [Stratton 86]. Apart from the angles of incidence at the grating the dimensions of the two SPREDs are identical. The 2105 g/mm grating is designed to operate at an angle of incidence which is 1.3° larger than that used for the 450 g/mm grating, 70.6°, in order to obtain reasonable signal strengths down to 100 Å. The entrance slits are 25 μm wide and 2.5 mm high. A baffle between the entrance slit and the grating restricts the ruled area of the grating used to 3 mm × 18 mm. An additional baffle between the grating and the detector provides a screen against possible wall reflections. The spatial resolution of the spectrometers in the poloidal direction of the

tokamak is given by the effective grating dimension and the ratio of the grating, entrance slit separation to the distance between the divertor and the entrance slit. The latter is about 6.8 m which results in a spatial resolution of $\approx$ 110 mm.

2.4. Detectors

Both SPREDs are equipped with a combination of a micro-channel plate (MCP) image intensifier [Wiza 79] and a phosphor screen coupled to a 2048-pixel linear photo diode array (PDA, Princeton Instruments Inc.) by a fiber-optic image conduit. The MCPs are of the high output technology type (HOT, Galileo Electro Optics Corporation), which are designed to produce a high output current. This results in an extended linear response and an increased dynamic range. A CuI coating on the irradiated surface of the MCP, in combination with funneled channels (biased by 8°), provides a substantial increase in detection efficiency. The diameter of the MCP channels is 10 μm and their center to center distance is 12 μm, which is less than the 25 μm pixel width of the PDA.

The MCP-phosphor assembly can be operated in two modes. In the first the MCP output is grounded and up to -1 kV is applied to the input, while the phosphor has a positive potential, typically 4 kV. In this case the MCP is sensitive to photons and (positive) ions. This can have the disadvantage that, if, for instance, ion gauges are used to monitor the spectrometer vacuum, occasional intensity spikes occur due to the detection of ions from the gauges. This problem can be avoided by operating the detector in the electron and photon detection mode. Grounding the input of the MCP and applying up to +1 kV to the output makes the MCP insensitive to positive ions. The positive phosphor potential then has to be increased by the output MCP voltage. As would be expected, the two modes exhibit the same sensitivity to VUV photons. At present, ion gauges are not being used on the spectrometer and the positive ion mode is regarded as the safer option. It has been used for the results described in this paper. This mode avoids any possibility of the voltage between the MCP and phosphor being raised to 5 kV as would happen if the MCP alone were to trip in the electron mode with the present electronic circuits. It should be noted that no evidence of spikes due to positive ions coming from the plasma has been found.

The PDA detectors consist of two 1024-diode arrays (Reticon RL2048S), each diode being 25 μm wide and 2.5 mm high, the full array having twice the width of the previously used diode arrays in the SPRED instruments. The spectral resolution, which is largely determined by the charge spreading between the MCP and phosphor screen (see section 3.3), remains unchanged and the present arrangement increases the number of array pixels in a spectral feature by a factor of 1.6. This has been achieved without any loss of information that would result from a 'dead space' between the two diode arrays. In combination with an MCP having an active area of 52 mm diameter and a straight fiber-optic conduit, the increased width of the PDA allows a 51.2 mm wide area of the dispersion plane to be imaged onto the detector, instead of the 40 mm flat focal field used in earlier SPRED designs. Consequently the spectral coverage is increased by more than 300 Å to 180 - 1500 Å for the 450-SPRED and by over 50 Å to 140 - 440 Å for the 2105-SPRED. An increase in aberrations, which would result in a loss of spectral resolution towards the ends of the observed spectra, has only been found for the 2105 g/mm grating (see section 3.3). The detector positions can be moved in the focal plane so as to change the spectral coverage, the adjustment being ~50 and 250 Å in either direction for the 2105- and 450-SPREDs, respectively. The analogue signals are digitized by a single 16 bit analogue to digital converter with a readout speed of 5 μsec/pixel; this results in a minimum readout time of just under 11 msec per spectrum.

2.5. Control system

The diagnostic is controlled by a computerized system which uses an interactive application program to adjust a number of parameters. An operator machine interface is provided via a local control panel as well as on the JET UNIX system in the main control room. The facilities include the display of the status of the high vacuum system, the monitoring and sequencing of the high voltages applied to the detectors, the setting of the detector timings and in future the positioning of the instrument's line of sight.

Some of the hardware of this system is situated near the instrument in the torus hall, while control cubicles containing further diagnostic specific hardware are situated

some 50 meters away in the easily accessible diagnostic hall, which is outside the biological shield. An Ethernet link provides a connection to the main control room, which is a further 100 meters away. Fig. 4 gives an overall view of the system.

A novel fiber optic field bus control system (Beckhoff Industrie Elektronik) is used. This is based on a 2.5 Mbit/sec inter-connect, to which different types of input/output (I/O) modules can be attached. In the present application, digital I/O, analogue I/O, position encoders and RS232 connections to stepper motor controllers are all used. The main advantage of the fiber optic field bus control system is that it employs a single fiber loop for data transfer which is independent of the type or number of modules, this minimizing the cabling requirements.

A high voltage controller (Caen SY127) provides full computer control of the high voltages applied to the spectrometer detectors, so that they can be set and monitored by the system software. High speed trip circuits ensure good protection of the detectors, while remote resetting of the trips via the control software enables a smooth recovery of the detector voltages to be achieved.

These two sub-systems are controlled by modules in a VME bus based crate with a Motorola 68040 processor, 8 Mbytes of memory, an Ethernet connection and real time clock facilities. The crate controller communicates with these modules by dispatching four byte datagrams to the modules at a frequency suited to the response time required by the system. Typically, the modules are accessed by the crate controller every 5 msec.

The real time operating system (VxWorks), with its TCP/IP support, provides messaging facilities to enable an interface with the control room. The main application software consists of a number of processes, each supporting a major function such as high voltage control or message routing. On the control room computer system a UNIX daemon process, developed for this application, forwards the requested settings into the system data base, as well as supporting Xwindow based mimics and touch panels for the operation of the diagnostic.

The spectral data is collected locally on a PC using standard Windows based software. After each pulse the data is sent to a central PC server, which communicates with the central JET data acquisition systems.

3. Performance

3.1. Gain Characteristics

The gain characteristics of the MCPs and phosphor screens have been measured using a hollow cathode light source (McPherson, model 629) [Paresce 71], this source producing steady state line emission. Using He for the discharge, the 304 Å, HeII line was chosen for the determination of the dependence of the sensitivity on MCP and phosphor voltage. Fig. 5 shows the normalized MCP gain characteristics. The reproducibility of independent measurements for each spectrometer is better than 5% for voltages above 800 V. Data from different regions of the MCP give the same results. It should be noted that the absolute gains of the two MCPs are different. The MCP gain of the 450-SPRED given by the manufacturer is 28 times that of the 2105-SPRED. However, a comparison between the two SPREDs, made using the 304 Å HeII-line emitted by the hollow cathode source run with identical discharge parameters, gave a factor of 18 and cross calibrations performed during plasma operations indicated that this factor has fallen to ~4. These comparisons include the effect of the gratings and other detector components. The observed change may be an indication of the MCPs being progressively conditioned.

The MCP gain characteristics can be described by the following power laws:

$$\text{450-SPRED:} \quad G_{MCP} = 4.812 \times 10^{-46} U_{MCP}^{15.144} \tag{1}$$

$$\text{2105-SPRED:} \quad G_{MCP} = 2.177 \times 10^{-37} U_{MCP}^{12.216}, \tag{2}$$

where the MCP voltage, U_{MCP}, is in volts. The MCP gain characteristic of the single SPRED spectrometer installed on JET with a horizontal viewing line for the observation of the bulk plasma is similar and can be described by the same power law [Hawkes 93]. This is also presented in fig. 5.

The gain characteristics of the phosphor screens, measured by the same technique, is presented in fig. 6. Only a small variation is found between the two SPRED detectors. In contrast to the MCP gain, which changes by orders of magnitude over the voltage range of interest, the phosphor gain has a relatively weak dependence on voltage. It is best approximated by a second order polynomial:

$$\text{450-SPRED:} \quad G_{PS} = 9.93 \cdot 10^{-4} - 5.81 \cdot 10^{-5} U_{PS} + 7.73 \cdot 10^{-8} U_{PS}^2 \qquad (3)$$

$$\text{2105-SPRED:} \quad G_{PS} = 9.68 \cdot 10^{-2} - 1.74 \cdot 10^{-4} U_{PS} + 1.00 \cdot 10^{-7} U_{PS}^2 \qquad (4)$$

This highlights the need for a high MCP voltage to give an overall gain factor close to the maximum possible. So as to avoid risking electrical breakdown, voltage limits for the JET double SPRED are set at 1 kV for the MCPs and 4 kV for the phosphor screens. For the latter, the limit is determined by the separation of the MCPs and phosphor surfaces.

3.2. Wavelength Calibration and Spectral Dispersion

Empirically, the wavelength calibration is determined by fitting a smooth function to the pixel position of a number of spectral lines of known wavelength. The usual choice of function is a power series or Chebyshev polynomial. The advantage of the latter is that the absolute magnitude of subsequent terms in the series decrease more rapidly than in a power series polynomial. The use of a Chebyshev polynomial is therefore more efficient in that fewer terms are needed to obtain a certain accuracy. It also avoids the danger of an oscillating fit that can occur when too high a degree of power series polynomial is fitted to a limited number of data points.

However, to acquire information about the accuracy of the alignment of the spectrometer, an analytical description is required. In fig. 7 a schematic diagram of the optical arrangement of the SPRED spectrometer is presented. The flat focal field lies between points B1 and B2 and the detector can be moved in the x-direction. The dependence of the wavelength on the angles of incidence and diffraction, α and β, respectively, is given by the grating equation,

$$k\lambda = \frac{1}{N}(\sin\alpha - \sin\beta), \qquad (5)$$

where k is the diffraction order and N the groove density. Considering a projection of the PDA onto the plane of the flat focal field, if x_0 is the position of the first pixel of the detector,

$$x = x_0 + p\,\Delta x\,. \qquad (6)$$

Δx is the width of a pixel projected onto the flat focal field. Since a straight fiber conduit is used, $\Delta x = 25\ \mu m$. Expressed in terms of the diffraction angle, β, x becomes

$$x = l_H \tan(\beta_H - \beta)\,. \qquad (7)$$

Consequently,

$$\lambda(p) = \frac{1}{k\mathrm{N}}\left(\sin\alpha - \sin\left(\beta_H - a\tan\left(\frac{x_0 + p\Delta x}{l_H}\right)\right)\right). \qquad (8)$$

This relation, fitted to experimental values of λ(p), can be used to confirm some of the geometrical measurements of the spectrometer. Since the detector can be moved along the x-axis, x_0 must be a free parameter. The choice of the other free parameters is arbitrary. The best fit is achieved by using three free parameters; using more does not improve the accuracy of the fit. In fig. 8 the fitted functions derived using x_0, α and β_H as free parameters are shown as well as their residuals. Expressed in terms of the pixel width, the residuals for both gratings are $\lesssim$ 1 pixel; the spectral resolution is ~5 pixels (see section 3.3). In table 1 the derived values of the free parameters are compared to their design values given by the grating manufacturer. The very small deviations ($\leq 0.2^\circ$ for the angles) emphasize the high accuracy achieved in the alignment of the grating and the detector. A second order Chebyshev polynomial was found to give a comparable accuracy to that of the analytical function and the use of higher order terms did not improve the accuracy.

The spectral dispersion is given by the derivative of eq. (8)

$$\frac{d\lambda}{dp} = \frac{1}{kN}\frac{l_H\,\Delta\mathrm{x}}{l_H^2 + (x_0 + p\,\Delta\mathrm{x})^2}\cos\left(\beta_H - a\tan\left(\frac{x_0 + p\,\Delta\mathrm{x}}{l_H}\right)\right). \qquad (9)$$

The dispersion can be evaluated using the parameters obtained from the fit to equation 8 and is plotted in fig. 9. The experimental data points are obtained by dividing the wavelength difference of neighboring lines by their pixel difference, this resulting in some scatter around the calculated curve.

3.3. Spectral Resolution

By far the most important contribution to the spectral line shape in spectra recorded with the SPRED spectrometers is the instrument function [Lawson 88]. This depends critically on the illumination of the grating. The hollow cathode source used for testing the spectrometer does not fill the acceptance angle of the spectrometer and, consequently, results in a narrower line profile than when an extended source, such as the JET plasma, is employed [Fonck 82, Stratton 86]. Because of this, the latter has been used to determine the spectral resolution and its dependence on wavelength.

The spectral lines utilized are selected so as to avoid line doublets or other line blends which would result in spuriously broad lines. Since many lines are found in the VUV spectral region and the spectral resolution is limited, particularly for the 450 g/mm grating, it is still possible that the chosen lines originate from more than one atomic transition. The presented spectral resolution therefore represents an upper limit. A line fit is performed using a formula which can represent either a Gaussian or Lorentzian function [Fraser 70], this depending on a profile parameter, α,

$$F(p) = \frac{1}{\left(1 + (2^{\alpha^2} - 1)\left(2\frac{p - p_0}{\Delta p_{1/2}}\right)^2\right)^{1/\alpha^2}}, \qquad (10)$$

where $\Delta p_{1/2}$ is the FWHM in pixels. As α is varied, F(p) changes continuously from a Gaussian ($\alpha \rightarrow 0$) to a Lorentzian profile ($\alpha = 1$). Fig. 10 shows the dependence of α on the line width. It can be seen that the values of $\Delta p_{1/2}$ and α for the 450-SPRED lie in a narrower range than for the 2105-SPRED. In both cases the profile is closer to that of a Gaussian than Lorentzian, for the 2105-SPRED almost reaching a pure Gaussian shape at the shortest wavelengths, where the line width is narrowest. It should be noted that the line wings are much less pronounced than was found previously for the single SPRED instrument [Lawson 88]. Since the line shape changes, the line width alone is an inadequate measure of the spectral resolution. This is defined according to the Rayleigh criterion as the separation between two neighboring lines of equal intensity sufficient for their summed intensities between the lines to fall to 80 % of the peak values. The fitted line widths are converted into a

spectral resolution using a factor, ~1.13, which depends weakly on α, determined by applying the criterion to the formula of equation 10.

The spectral resolution is shown as a function of wavelength in fig. 11 and is comparable to the values found for other SPRED spectrometers [Brzozowski 91]. The measured spectral resolution for the 450-SPRED shows no clear dependence on wavelength and certainly there is no loss of resolution due to the extended focal field used in the present instrument. In contrast, there is evidence of some deterioration in the resolution above 350 Å for the 2105-SPRED. This wavelength corresponds to the end of the flat focal field. The spectral resolution for the 2105-SPRED is a factor ~4 better than that of the 450-SPRED.

The spectral resolution also depends on the voltages applied to the detectors. The most significant component to the instrument function is due to the charge spreading in the gap between the phosphor and the MCP. The effect on this spreading of varying the voltage can be marked; for the double SPRED detectors a broadening of the line width of the hollow cathode light source of up to 40% is observed when the phosphor voltage is reduced from 4 to 0.5 kV. In addition to this voltage dependence, the charge spreading increases with the separation between the MCP and phosphor surfaces. Given that a high phosphor voltage is required to maximize the gain factor, the operating parameters have to balance the requirement of a high resolution and gain factor without risking electrical breakdown. Consequently, the detectors are operated at a voltage of 3.5 to 4 kV with a fixed MCP-phosphor gap of 0.75 mm. Reducing the MCP voltage from 1000 to 650 V results in a small improvement in the resolution of about 5%. A possible explanation is space charge effects on the electrons leaving the MCP-channels.

3.4 Detector Shielding

An important aspect of the spectrometer design is the stainless steel shielding used to reduce nuclear radiation-induced background counts during high performance plasma discharges. Fig. 12a and 12b illustrates spectra observed during such a discharge with the unshielded, single SPRED and the double SPRED instruments, respectively. In

both, the 450g/mm gratings were used to record the spectra, which are shown for a time of 13.3s, this being close to that of the peak neutron emission. The discharge, pulse 34230, has D as the fuel and is heated by D neutral beam injection (NBI), reaching a neutron yield of $4.1 \times 10^{16} s^{-1}$. It should be emphasized that the difference between these spectra is enhanced by the respective intensity of their spectral lines. As will be discussed in section 4, those observed with the single SPRED with its horizontal line of sight are comparatively weak when diverted plasmas are configured, while the divertor plasma viewed by the double SPRED gives rise to particularly intense VUV emission. The figures are drawn with the same scale, the intense lines in fig. 12b being truncated.

In the spectrum from the single SPRED spectrometer, figure 12a, three effects can be seen. The first is a general rise in the background counts at all pixels, secondly, some broader features rising above this background and, finally, a number of narrower spikes. It should be noted that in this spectrum, there are only 6 features that can be identified with spectral lines, all falling to short wavelengths. The other broad features appear for only a single scan at positions which change randomly from scan to scan. Their width which is comparable to that of the instrument function would suggest that they are due to neutrons and γ rays interacting with the MCP of the detector. This is because the instrument function is largely due to the spreading of the electrons between the MCP and phosphor. Indeed the general rise in the background level is thought due to the occurrence of a large number of these events. There are also a number of spikes narrower than the instrument function, which can only come from the phosphor or subsequent detector components. These spikes add to the general level of noise, but on the whole appear to be comparatively small. A few of the most distinct single and double pixel spikes are indicated in figure 12a. In figure 12b showing the spectrum of the shielded double SPRED instrument, the background rise is less severe. However, a general increase in the noise level and narrow spikes are observed.

Of most concern, therefore, is the interaction of neutrons and γ rays with the MCPs; it is noted that this is a bulk effect, rather than the surface effect that occurs for the VUV photons. In contrast to the γ rays, which can lead to the direct emission of electrons in the MCP, the neutrons are thought to generate electrons via a secondary process, from

the ionizing radiation produced by such reactions as (n,p) or (n,α) or from the recoil motion of the heavy nucleus in such reactions. The available data suggests that the MCP response is about 5 to 10 times higher to γ rays than to neutrons [Timothy 79, Medley 81].

The bulk of the neutrons reaching the spectrometer detectors are expected to come directly from the plasma DD reactions in the high ion temperature region near the plasma center and will therefore have an energy of about 2.45MeV. In general, providing RF additional heating is not used, the direct γ ray emission from the plasma is expected to be much smaller than the more isotropic secondary emission resulting from neutron collisions with the various machine structures.

Steel is an efficient attenuator of both γ rays and neutrons, if the latter have energies above the inelastic scattering threshold of 0.86 MeV. For example, 15 cm of steel reduces the neutron flux by a factor ~8 and that of 8 MeV γ rays by a factor of ~17 [Avery 91]. Such reductions were thought worthwhile and a design was chosen enclosing the detectors in a shielding having 15 cm thickness of stainless steel in a direct line of sight to the plasma and 5 cm to the sides and back. This is shown in figure 1, although only the 15 cm shielding is illustrated in figure 3. In addition, materials which can act as a neutron moderator, such as those that contain hydrogen, have been avoided, so as to minimize the secondary γ ray emission that might result from slowing the neutrons to energies at which the capture cross-section is high.

A check was made on the effectiveness of the shielding by comparing the increase of the backgrounds in spectra observed with the double SPRED and the unshielded, single SPRED instrument during two high performance discharges. Both were D discharges, pulses 34230 and 34496, heated by D NBI and reaching neutron yields of 4.1 and $3.6 \times 10^{16} s^{-1}$, respectively. The spectra for the former pulse are shown in fig. 12. Once the difference in detector gains are accounted for and a small correction is made for the greater distance of the single SPRED detector from the plasma center, 5.65m as opposed to 5.00m for the double SPRED, the comparison suggests that to within a factor of 2, the background is ~7 times lower for the shielded double SPRED instrument. This is a valuable improvement, allowing a more reliable interpretation of the spectra, and is of the order of magnitude that might be expected from the initial design estimate. Further experiments are planned to investigate whether the

improvement is due mainly to the attenuation of the direct neutrons or from the secondary γ rays.

4. Diagnostic Applications and First Experimental Results

The double SPRED spectrometer has been commissioned during the 1994 JET plasma operations and is now routinely used in the study of the divertor plasmas produced in the upgraded JET machine. The diagnostic provides valuable data that will aid the analysis of the impurity transport in the divertor region. Some initial results are presented which illustrate the quality of the data being recorded. These were obtained with a near-vertical, fixed line of sight viewing the divertor target tiles close to the inner strike zone of the plasma, which has an X-point configuration.

Typical examples of spectra recorded with the double SPRED spectrometer are shown in fig. 13. These observations were made at 16.3 s in JET pulse 32779. The two spectra from the double SPRED instrument, covering wavelength ranges of 140 to 440 Å and 180 to 1490 Å, figs. 13a and 13b respectively, are compared with that recorded with the single detector SPRED instrument, fig. 13c, which has a near horizontal line of sight close to the vessel midplane. The grating with a groove density of 450 g/mm, with a wavelength coverage of 100 to 1100 Å, was used to record this latter spectrum. In the case of the bulk plasma, it is important to observe wavelengths down to 100 Å, since a number of important, high temperature lines occur in the 100 to 200 Å spectral region. In contrast, the 140 to 1490 Å range of the double SPRED instrument matches well the emission expected from the lower ionization stages present in the divertor, its plasma having a lower T_e than the bulk plasma. It can be seen in figs. 13a and 13b that the divertor spectra are dominated by the lower temperature emission and this contrasts with the bulk plasma VUV spectrum, fig. 13c, which contains spectral lines from a wide range of ionization stages characteristic of all regions of the plasma.

Although absolute sensitivity calibrations for the double and single SPRED instruments are not yet available, the latter having an upgraded detector since the last measurements [Hawkes 93] were made, a comparison of the relative intensities of

lines observed by each instrument can still be made. The highest ionization stage which can be seen in both instruments is Ni XXVI, this having the most poloidally symmetric emission. Using the 165 Å, Ni XXVI line, which can be clearly seen by both the single SPRED and the 2105-SPRED, together with estimates of the relative sensitivity calibration for each detector, comparisons are made for low temperature lines in the 300 to 1000 Å spectral range. This suggests that the spectral line intensities recorded along a vertical line of sight passing through the divertor region are typically a factor of ~40 higher than those viewed along a horizontal, midplane line of sight. This is attributed mainly to the higher n_e in the divertor plasma and to the higher density of low ionization states near the main recycling source. It clearly indicates that the dominant emission recorded by the double SPRED spectrometer is from the divertor region, despite the line of sight passing through the whole of the bulk plasma.

The shortest exposure time, which enables the full spectral range to be read, 11 msec, gives sufficient time resolution to allow events such as Edge-Localized Modes (ELMs) to be resolved. ELMs are instabilities characteristic of the high confinement (H-) modes, in which there is a redistribution and efflux of particles resulting in a burst of D_α radiation from the recycling of the fuel species. This is illustrated in fig. 14 for pulse 32773, in which there is an ELMy H-mode. The fuel in this pulse is D and the figure shows the D_α trace recorded with a vertical line of sight viewing the outer edge of the divertor box, the time history being dominated by a sequence of ELMs. The behavior of the D_α is mirrored in the CII, CIII and CIV line intensities, fig. 14a, and those of OIII, OIV and OV, fig. 14b, observed with the double SPRED instrument. A difference can be seen between the short lived C features and those of O, which have a slower decay. Given the similarity of the ionization potentials of CIII and OIII, 48 and 55 eV, respectively, and of CIV and OIV, 64 and 77 eV, respectively, and that the impurity transport of C and O ions is not expected to differ significantly, the difference in the C and O time histories is attributed to the source of the impurities, reflecting a difference in their release mechanisms. C is released from the tile surfaces by physical sputtering, this process having a strong dependence on the

incident particle energy, whereas a chemical mechanism involving D is involved in the release of O.

For both elements, a subtler change is evident from one ionization stage to the next. This behavior may be explained by a spatial localization of the emission. Further evidence for such a localization can be found when the X-point is swept in order to spread the heat reaching the divertor tiles. To illustrate this, a period is chosen during pulse 32779, before the application of neutral beam heating. This begins at 15.5 s and is responsible for a significant rise in the CIV line intensity, at this time. In fig. 15, the top trace shows the major radius of the position of the inner strike point. The CII and CIII line intensities are clearly correlated with the strike point position and this pulse is exceptional in that they are out of phase with the CIV emission. This indicates that spatially resolved measurements are already obtained before a spatial scan of the divertor is made by rocking the instrument.

To illustrate the spectroscopic data which will allow impurity transport analysis of the divertor region and of the scrape-off-layer, a high performance H-mode pulse with a 0.6 sec ELM-free period is chosen as an example, pulse 32952. This is a 3 MA, D fueled discharge heated with 19 MW of D NBI. As shown in fig. 16, there is a transition to the H-mode regime within a few 100 msec of the onset of neutral beam heating. The line-integrated n_e, the stored energy and the DD reaction rate are seen to rise steadily up to the time of the first giant ELM at 13.1 s. A stored energy of 9 MJ is reached, at a maximum T_e of 12 keV, and a peak DD reaction rate of nearly $7x10^{16}$ sec^{-1} is achieved.

Emission from the bulk plasma is recorded with the single SPRED with its horizontal line of sight. The X-point magnetic configuration is formed after 11 s and it can be seen in fig. 17a that the CIV and OV emission falls to very low levels, in this case barely being measurable. A reduction in line intensity with the change of configuration from limiter to X-point is typical of the low Z species. The more central NiXXVI ionization stage is much less affected by the transition to X-point and is then seen to rise as n_e increases. The giant ELMs between 13.0 s and 13.6 s have a marked effect on the Ni and are seen as spikes on the CIV signal. In contrast, the low Z

emission from the divertor region measured by the double SPRED is more intense. Fig. 17b shows divertor CIII, CIV, OIV and OV intensities during the period in the H-mode phase that is free from giant ELMs. The similarity of the CIV and OIV time histories suggests that transport as well as local values of n_e and T_e, rather than the source term, are the dominant factors determining the divertor impurity behavior in this pulse, this contrasting with the ELMy H-mode discussed above (fig.14).

The capability of varying the line of sight of the double SPRED spectrometer to observe the whole of the divertor region will greatly enhance the analysis of the impurity transport within the divertor plasma. The availability of an absolute sensitivity calibration will allow measurements of the absolute fuel and impurity line intensities and enable the derivation of impurity density profiles and radiated power fractions within the divertor. Independent measurements of electron densities and temperatures will be possible from particular line pairs and the question of opacity in the JET divertor can be addressed by the simultaneous observation of deuterium Lyman and Balmer spectral features.

Acknowledgments

The authors would like to thank the continuous support and encouragement of P. R. Thomas during the strenuous task of installing and commissioning the double SPRED spectrometer and M J Loughlin for useful discussions in the preparation of this paper. They also wish to thank W. Studholme, B. Marshall, J.-L. Bonnerue and all the members of the diagnostic engineering group who were involved in the installation of the instrument, in particular J. Reid, A. Tiscornia, W. Spensley and O. J. Hancock for the days and nights spent in the torus hall. Finally we wish to thank the members of the JET vacuum group for their patience and support during the commissioning phase of the diagnostic.

References

[Avery 91] A. F. Avery, private communication (1991)

[Bertolini 95] E. Bertolini and the JET Team, Fusion Engineering and Design **30**, 53 (1995)

[Brzozowski 91] J. H. Brzozowski, E. Källne, K.-D. Zastrow, Physica Scripta **43**, 283 (1991)

[Carraro 89] L. Carraro, M. E. Puiatti, P. Scarin, M. Valisa, Proc. 16th Eur. Conf. on Controlled Fusion and Plasma Physics, Venice, Part IV, 1497 (1989)

[Carraro 93] L. Carraro, M. E. Puiatti, P. Scarin, M. Valisa, Proc. 20th Eur. Conf. on Controlled Fusion and Plasma Physics, Lisboa, Part II, 451 (1993)

[Fraser 70] R. D. B. Fraser and E. Suzuki, Spectral Analysis: Methods and Techniques, Marcel Dekker Inc. (1970)

[Fonck 82] R. J. Fonck, A. T. Ramsey, R. V. Yelle, Appl. Opt. **21**, 2115 (1982)

[Hawkes 93] N. C. Hawkes, K. D. Lawson, N. J. Peacock, UV and X-ray spectroscopy of Astrophysical and Laboratory Plasmas, Proc. 10th International Colloquium, Berkeley, California, Ed: E. H. Silver & S. M. Kahn, Cambridge University Press, 324 (1993)

[Janeschitz 90] G. Janeschitz, L. B. Ran, G. Fußmann, K. Krieger, K.-H. Steuer, Report IPP III/147, Max-Planck-Institut für Plasmaphysik, D-8046 Garching (1990)

[Lawson 88] K D Lawson, N J Peacock, Optics Communications **68**, 121 (1988)

[Medley 81] S. S. Medley, R. Persing, Rev. Sci. Instrum. **52**, 1463 (1981)

[Paresce 71] F. Paresce, S. Kumar, C. S. Bowyer, Appl. Opt. **10**, 1904 (1971)

[Schwob 87] J. L. Schwob, A. W. Wouters, S. Suckewer, Rev. Sci. Instrum. **58**, 1601 (1987)

[Stangeby 92] P. C. Stangeby, J. D. Elder, J. Nucl. Mater., **196**, 258 (1992)

[Stratton 86] B. C. Stratton, R. J. Fonck, K. Ida, K. P. Jaehnig, A. T. Ramsey, Rev. Sci. Instrum. **57**, 2043 (1986)

[Timothy 79] J. G. Timothy, R. L. Bybee, Rev. Sci. Instrum. **50**, 743 (1979)

[Walker 94] C. I. Walker, S. F. Dillon, N. P. Hammond, C. J. Hancock, N. Lam, E. J. McCarron, P. C. S. Prior, J. Reid, S. Sanders, X. Tellier, A. J. Tiscornia, G. A. H. Whitfield, C. H. Wilson, D. J. Wilson, Proc. 18th Symposium on Fusion Technology, Karlsruhe, 823 (1994)

[Wiza 79] J. L. Wiza, Nucl. Instrum. Methods **162**, 587 (1979)

[Wood 88] R. D. Wood, S. L. Allen, Rev. Sci. Instrum. **59**, 1537 (1988)

[Zastrow 93] K.-D. Zastrow, J. H. Brzozowski, Phys. Fluids B **5**, 4099 (1993)

Tables

Table 1. Comparison of the design values with those obtained from a least squares fit. The design value of x_0 has been calculated for the wavelength at which the experimentally determined scale starts.

	450 g/mm grating		2105 g/mm grating	
	Design	Fit	Design	Fit
x_0 (mm)	102.351	102.101	108.097	108.591
α (deg)	70.565	70.399	71.875	71.809
β_H (deg)	87.852	87.651	86.542	86.572

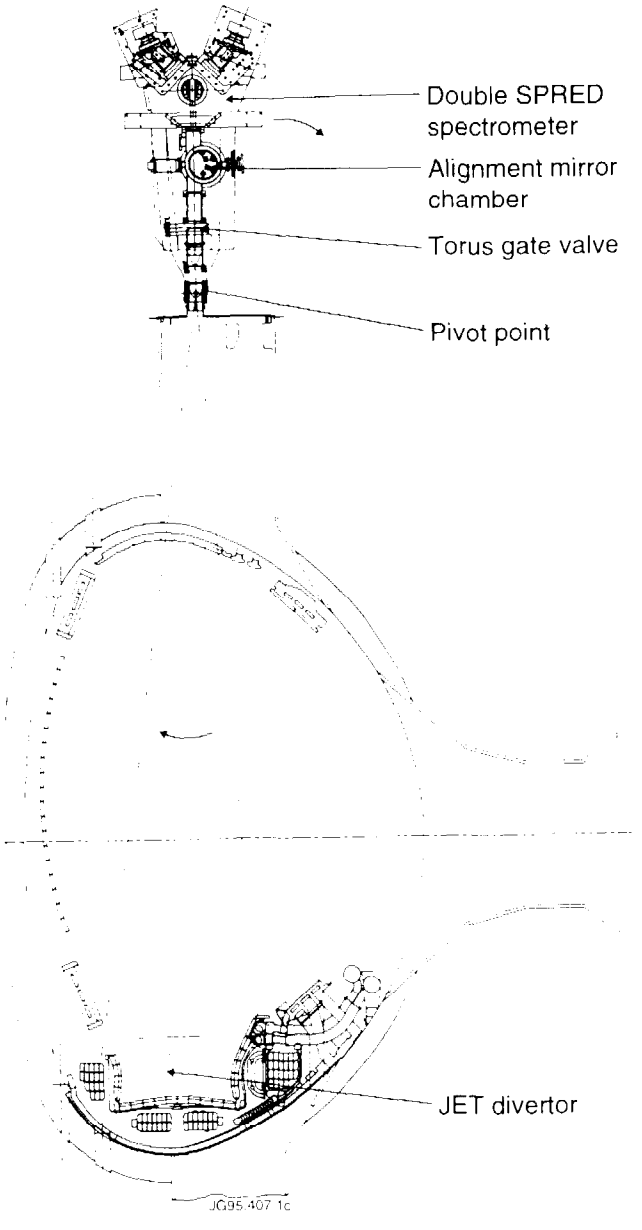

Fig.1. The experimental setup of the double SPRED spectrometer for the observation of the JET divertor plasma. Since no mirrors are involved in the spectrometer optics, the whole assembly is moved to change the viewing line position. The dashed lines indicate the possible spatial coverage of the divertor.

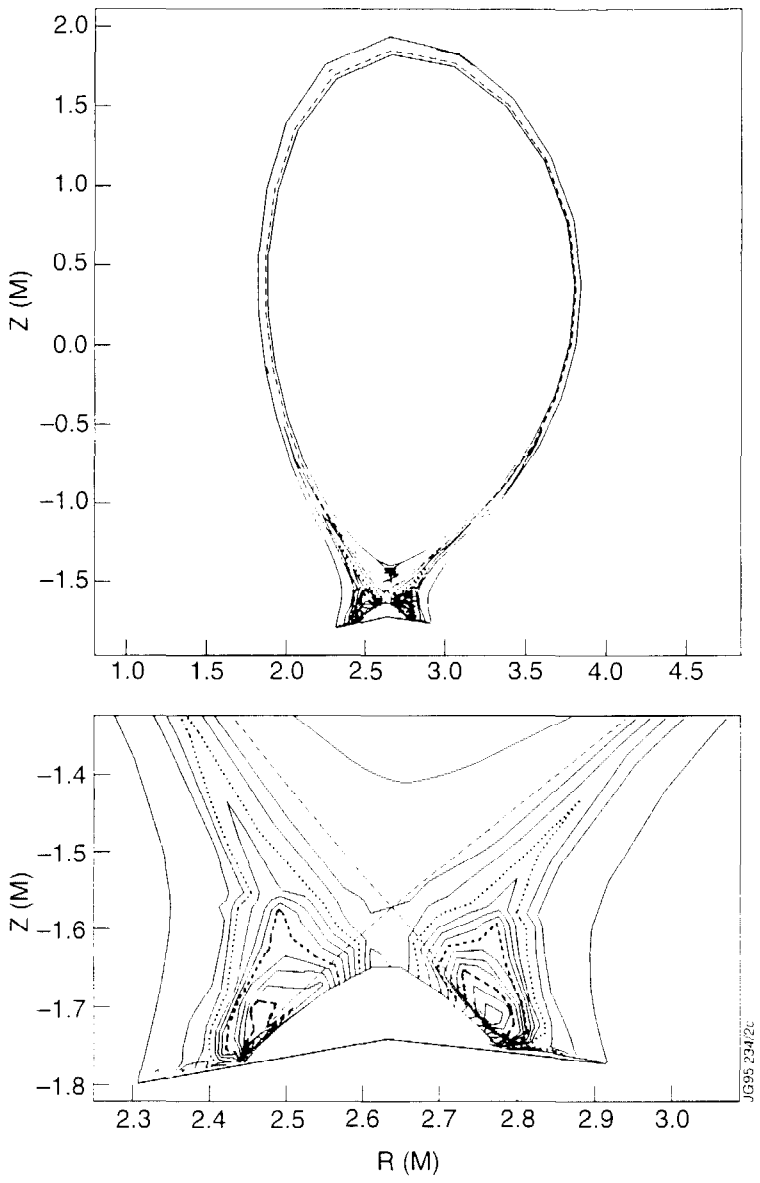

Fig.2. Simulated contours of the density of C IV ions in the JET (a) edge plasma and (b) divertor. This simulation was carried out for a divertor plasma with an electron density at the separatrix strike point of $5\times10^{19}m^{-3}$, an electron temperature of 5 eV, and an ion temperature of 15 eV.

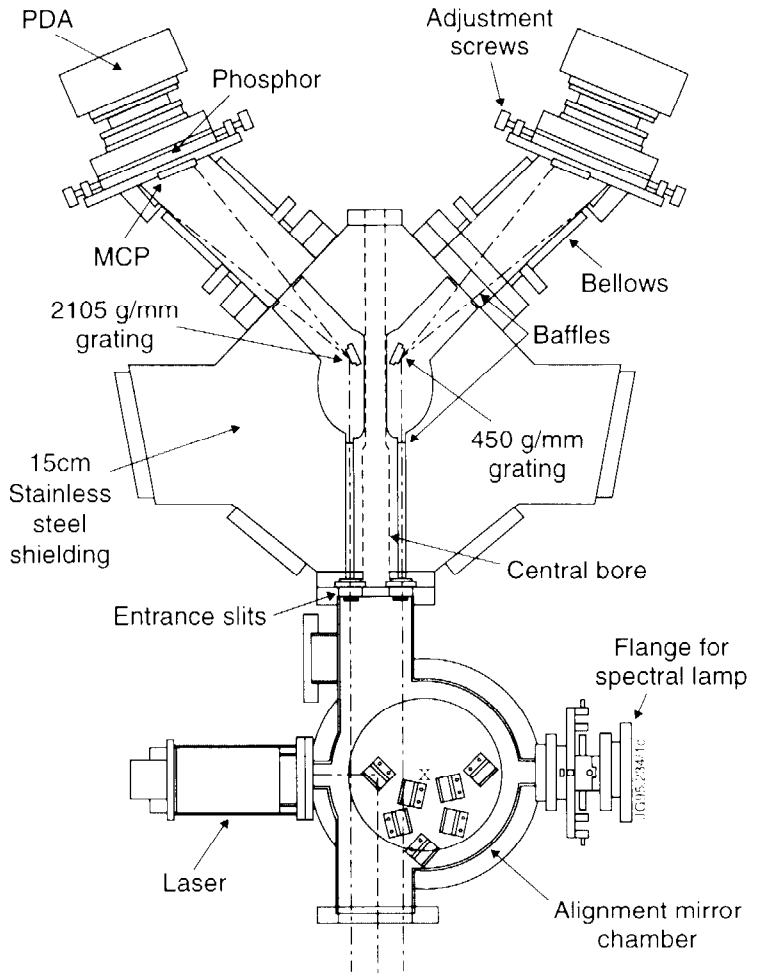

Fig.3. The double SPRED spectrometer and mirror chamber for the alignment of the spectrometer assembly. In the position shown, the rotary table directs a laser beam into the torus.

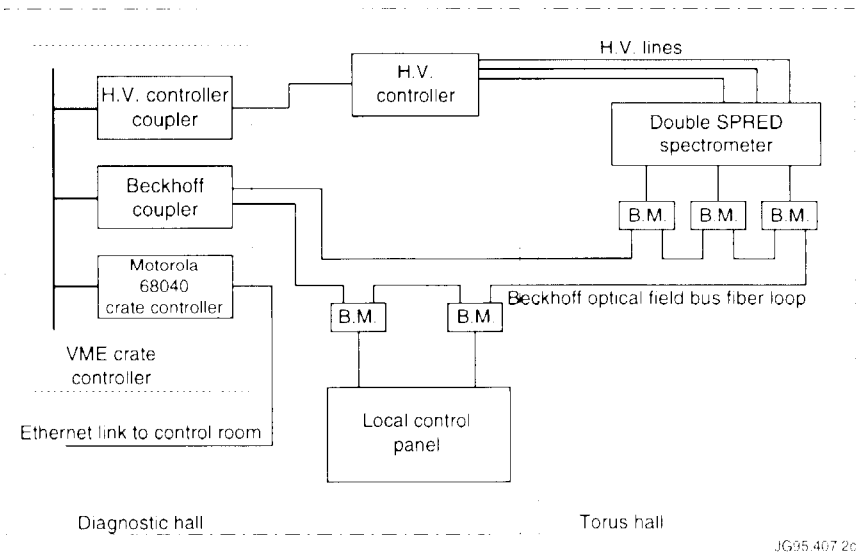

Fig.4 Overview of the diagnostic control system. The main components are the Beckhoff optical field bus control system with various I/O modules (B.M.) and the high voltage (H.V.) controller. A single fiber loop is required for all the I/O applications.

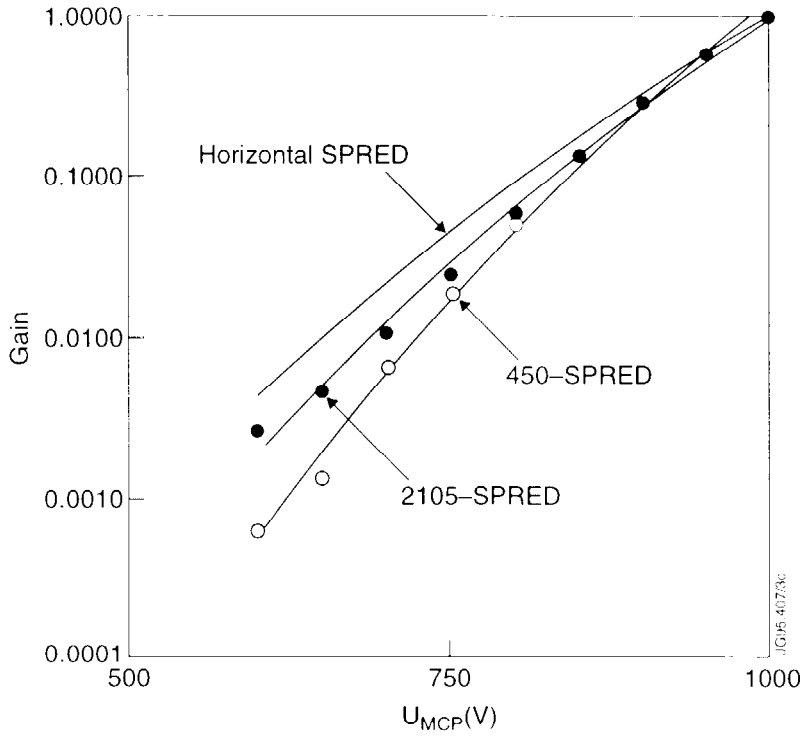

Fig.5. Voltage gain characteristics of the MCPs. The gain (normalized to that at 1000 V) is plotted against applied voltage. Measured data (• and ◦) are compared with the fit to a power law (solid lines). Also shown is the gain characteristic of the JET single SPRED which has a horizontal viewing line.

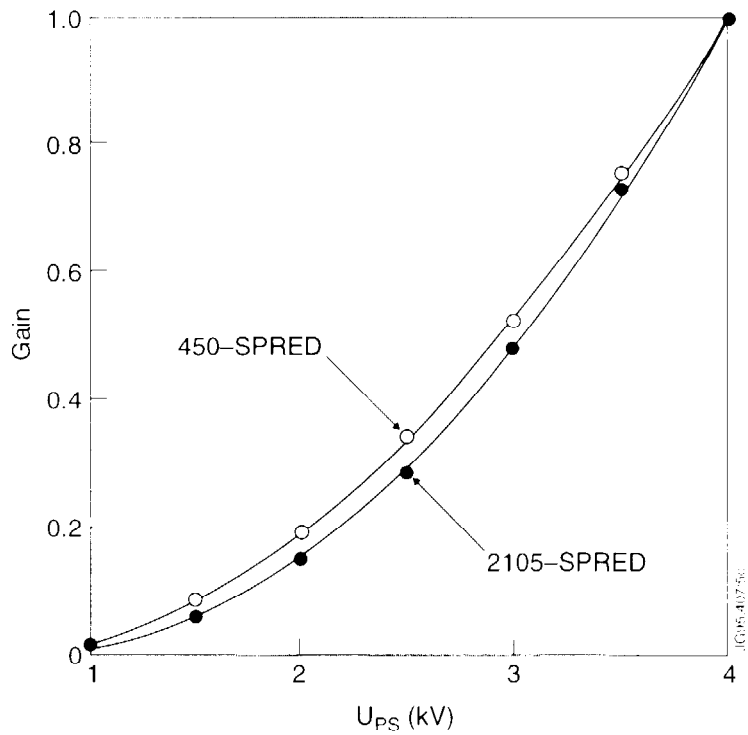

Fig.6. Voltage gain characteristics of the phosphor screens (PS). The gain normalized to that at 4000 V is plotted against applied voltage. Measured data (• and ◦) are compared with the fit to a second order polynominal (solid lines).

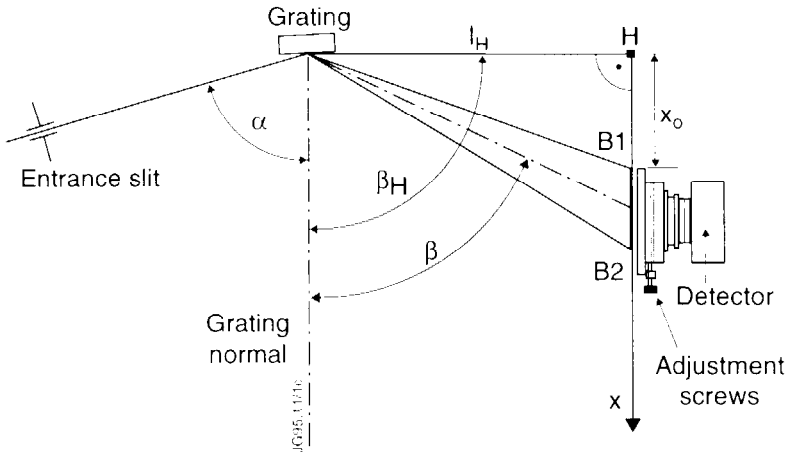

Fig.7 Schematic diagram of the optical arrangement of the SPRED spectrometer.

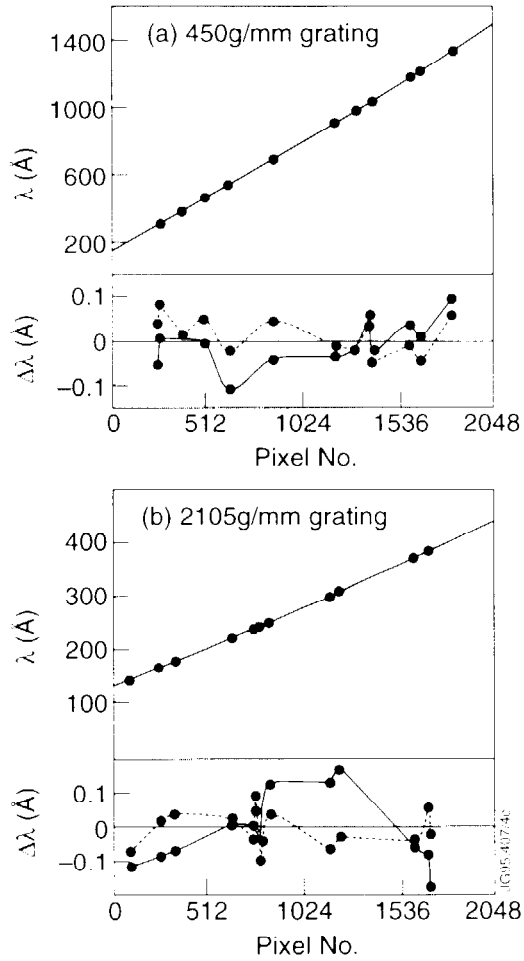

Fig.8. Wavelength calibration for (a) 450 g/mm grating and (b) 2105 g/mm grating. The experimental data (circles) are compared with the fit function. The residuals $\Delta\lambda$ are shown for the analytical description of $\lambda(p)$ (solid line) and a second order Chebyshev polynominal (dashed line).

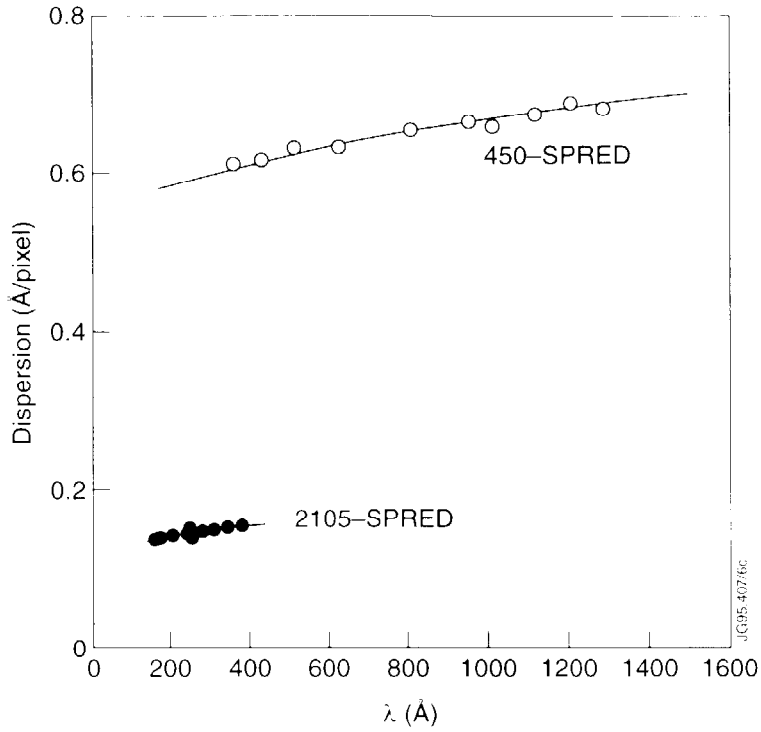

Fig.9. Spectral dispersion. Experimental data points (• and ○) and calculation from the derivative of the wavelength calibration.

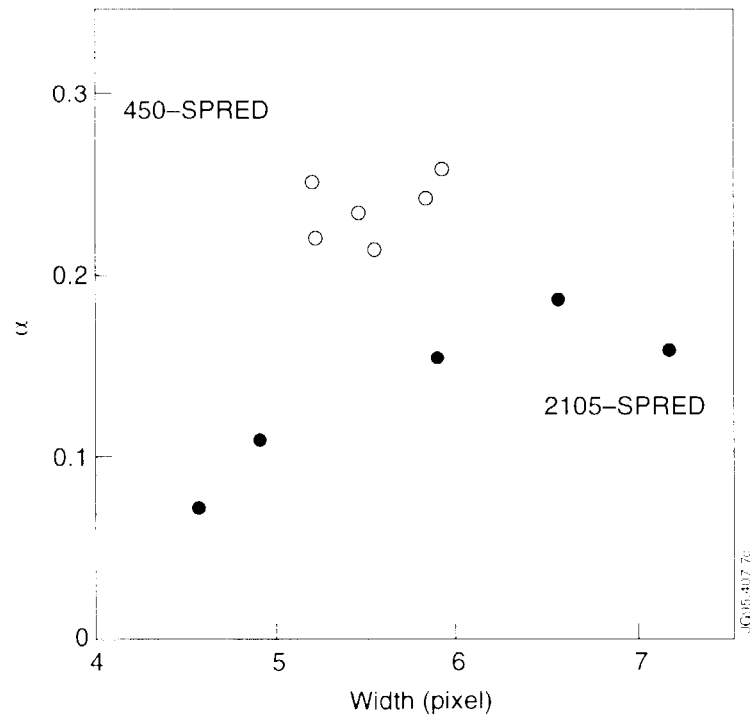

Fig.10. Dependence of the line profile parameter α on the line width. An increasing value of α corresponds to a change in the line shape from Gaussian to Lorentzian.

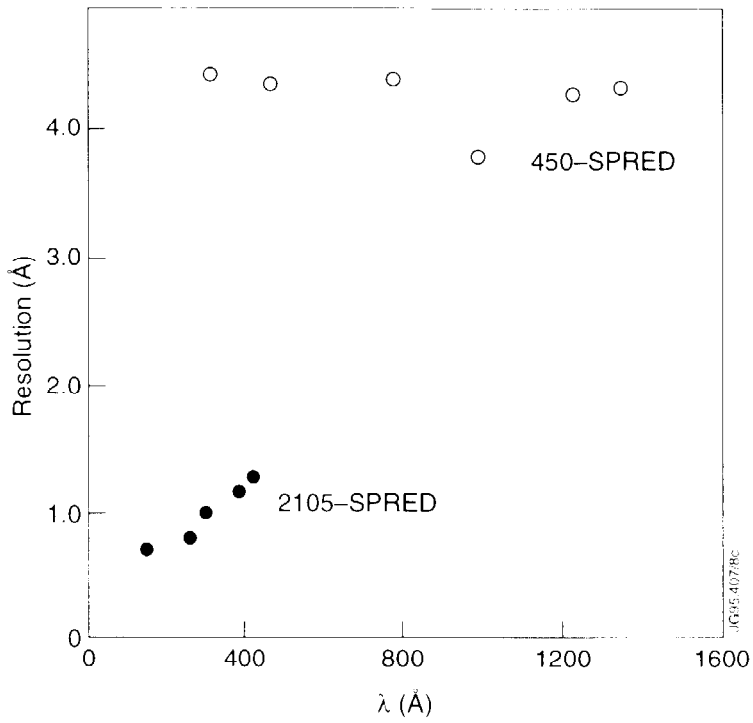

Fig. 11. The measured spectral resolution (• and ○) as a function of wavelength.

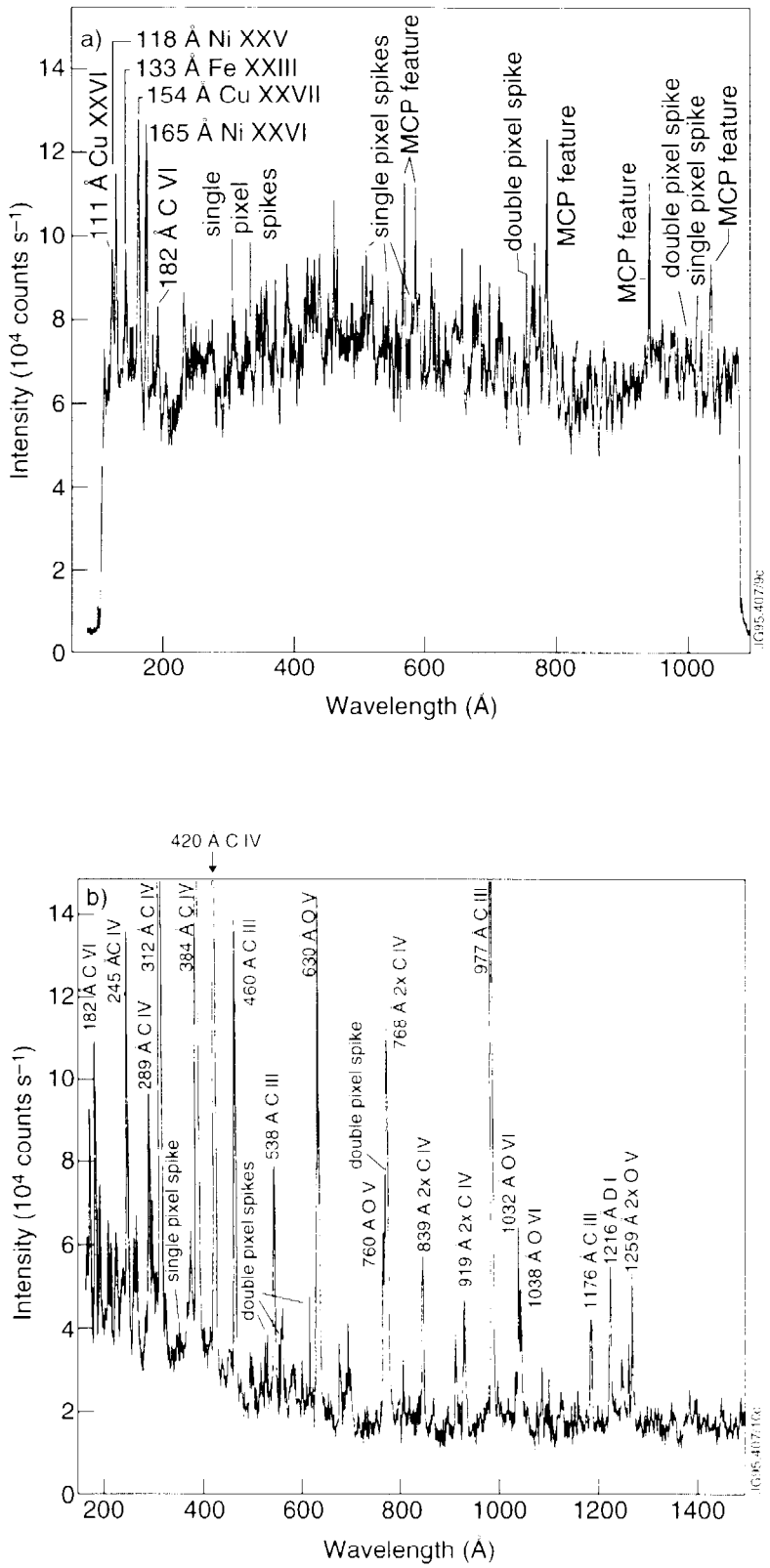

Fig.12. VUV spectra of (a) the bulk plasma viewed horizontally with the single SPRED and (b) the divertor plasma viewed with the double SPRED for the high performance discharge pulse 34230 at 13.3s, close to the time of the peak neutron yield, showing the increased backgrounds due to nuclear radiation-induced noise. The intense lines are truncated in (b).

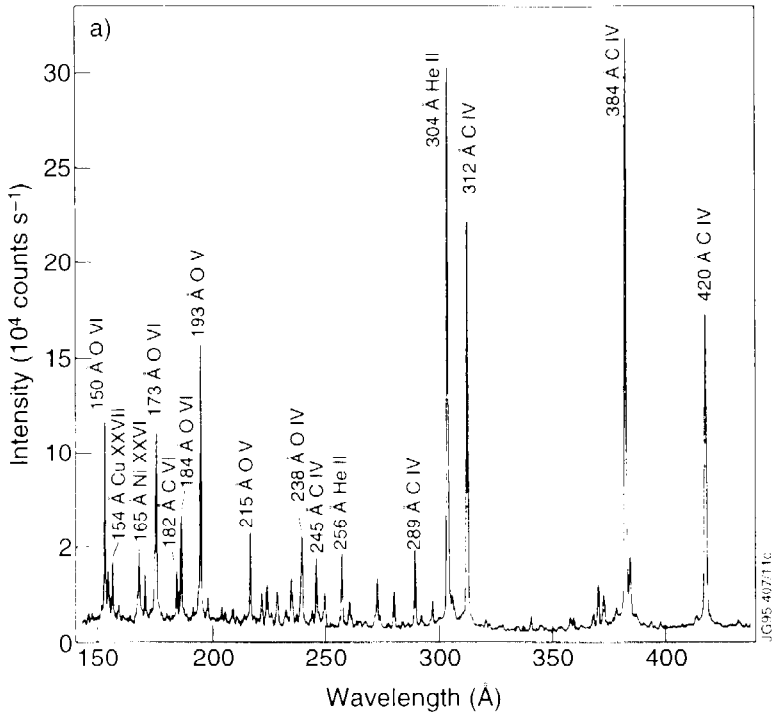
a)
Intensity (10^4 counts s^{-1})
Wavelength (Å)
150 Å O VI
154 Å Cu XXVII
165 Å Ni XXVI
173 Å O VI
182 Å C VI
184 Å O VI
193 Å O V
215 Å O V
238 Å O IV
245 Å C IV
256 Å He II
289 Å C IV
304 Å He II
312 Å C IV
384 Å C IV
420 Å C IV

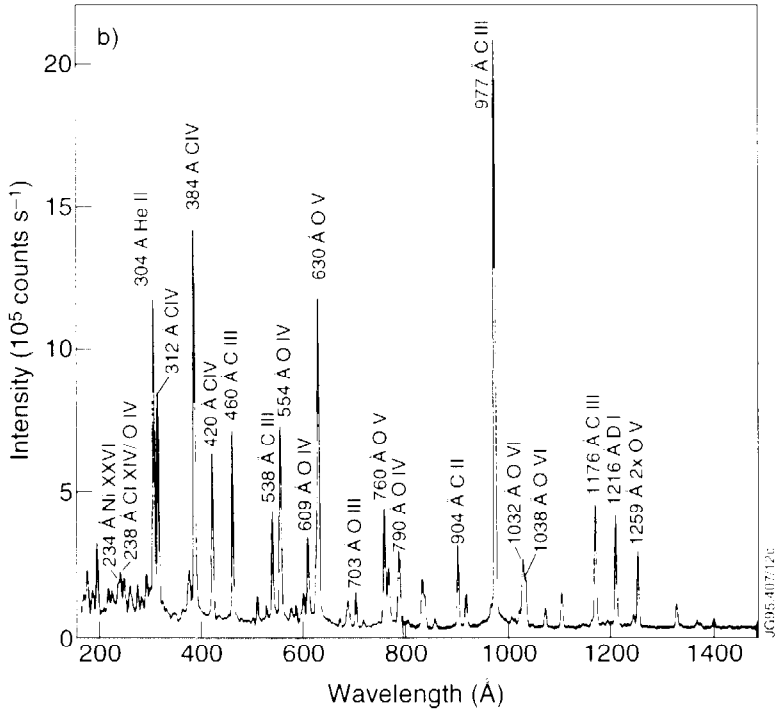
b)
Intensity (10^5 counts s^{-1})
Wavelength (Å)
234 Å Ni XXVI
238 Å Cl XIV/ O IV
304 Å He II
312 Å CIV
384 Å CIV
420 Å CIV
460 Å C III
538 Å C III
554 Å O IV
609 Å O IV
630 Å O V
703 Å O III
760 Å O V
790 Å O IV
904 Å C II
977 Å C III
1032 Å O VI
1038 Å O VI
1176 Å C III
1216 Å D I
1259 Å 2x O V

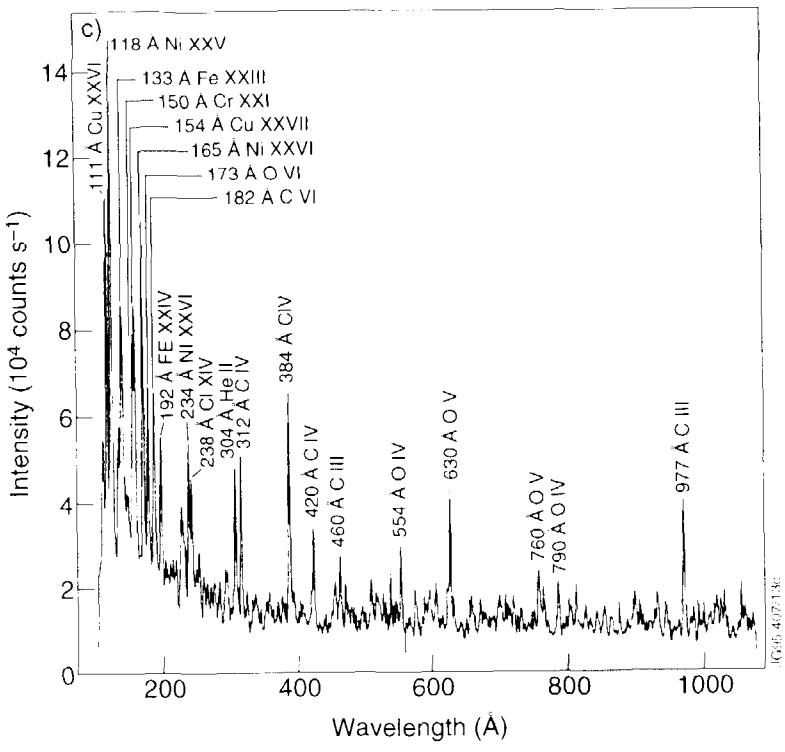

Fig.13. VUV spectra of the divertor plasma for pulse 32779 recorded at 16.3 sec with (a) the 2105 g/mm and (b) the 450 g/mm grating of the double SPRED spectrometer. (c) shows the corresponding spectrum of the bulk plasma viewed horizontally with the 450 g/mm single SPRED.

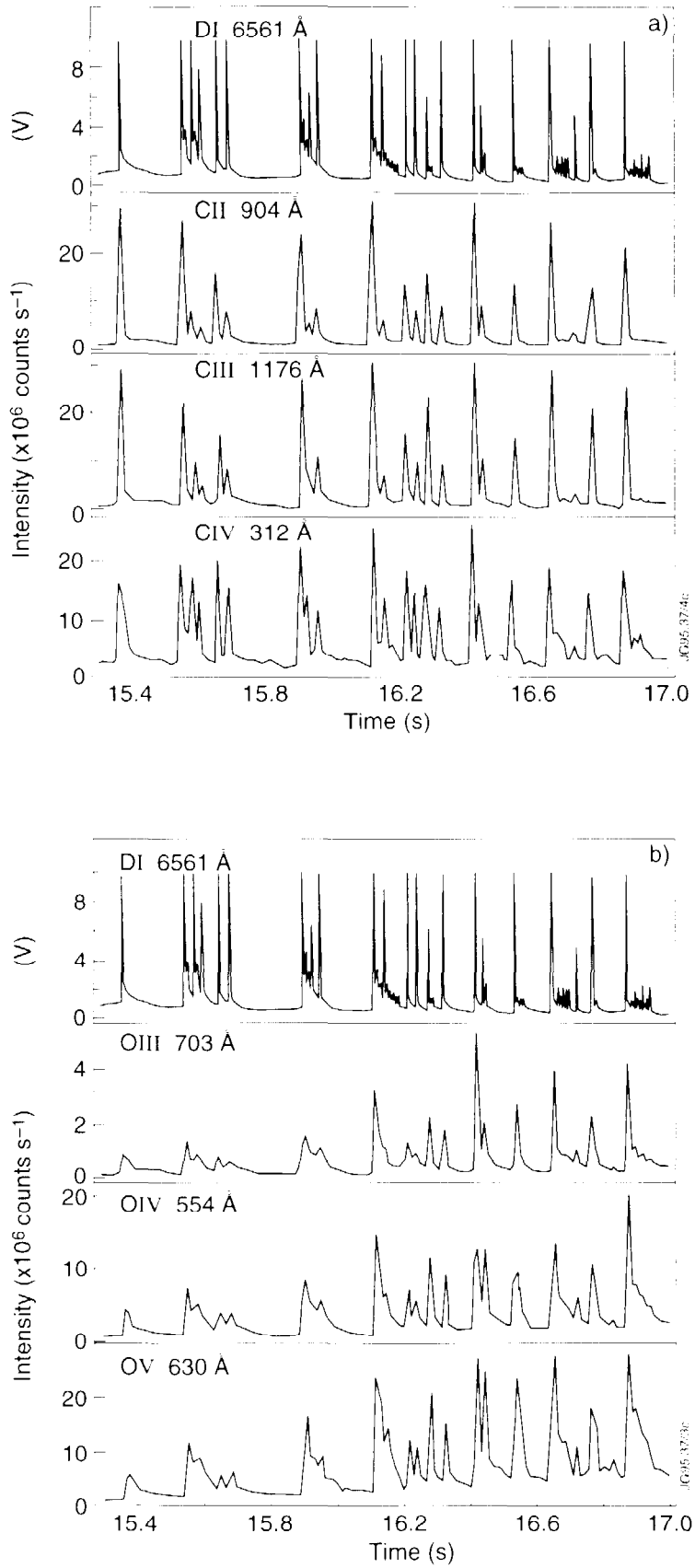

Fig. 14. D_α emission and (a) the CII, CIII and CIV and (b) the OIII, OIV and OV line intensities during the ELMy H-mode phase of pulse 32773 observed with the double SPRED spectrometer.

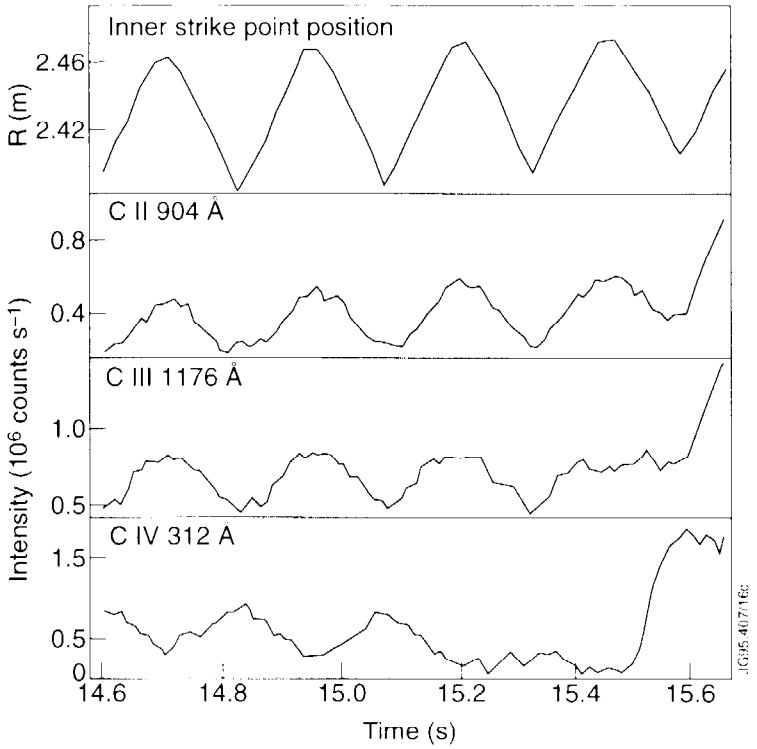

Fig.15. Carbon emission during the sweeping of the X-point position, which is shown in the movement of the major radius of the inner strike point.

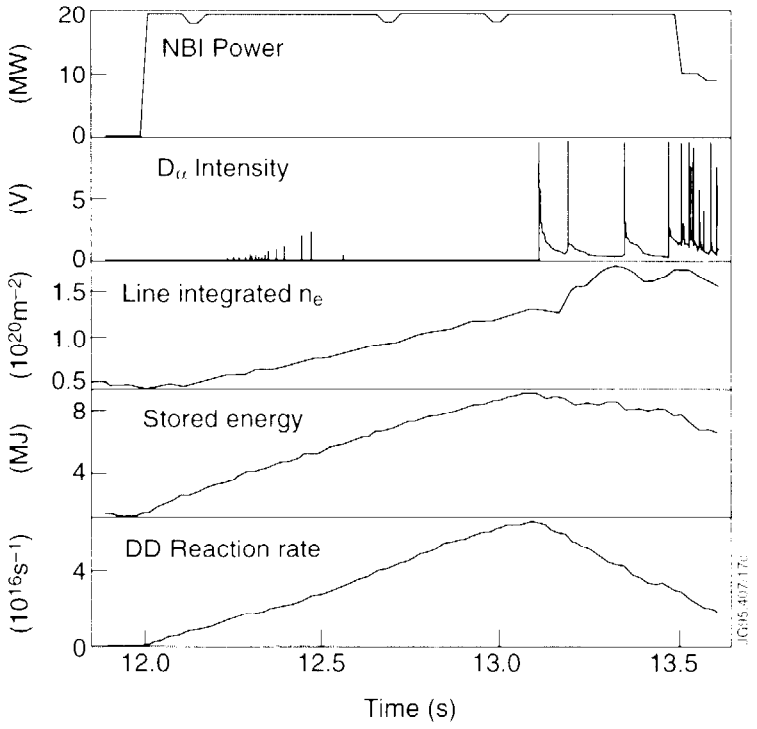

Fig.16. Additional heating power, D_α emission, line integrated n_e, stored energy and DD reaction rate for the high performance pulse 32952.

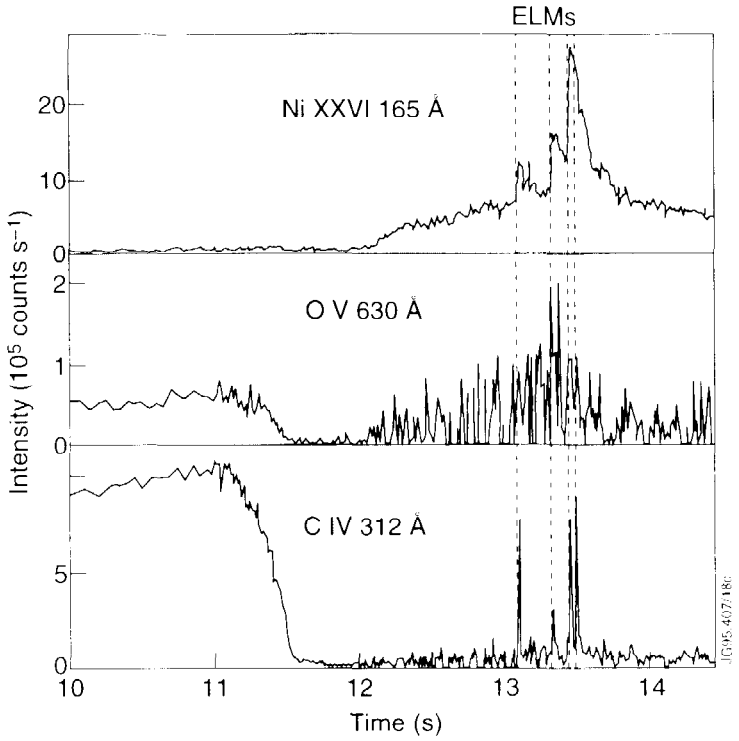

Fig.17a. CIV, OV and NiXXVI line intensities from the bulk plasma observed with the single SPRED spectrometer for the high performance pulse 32952.

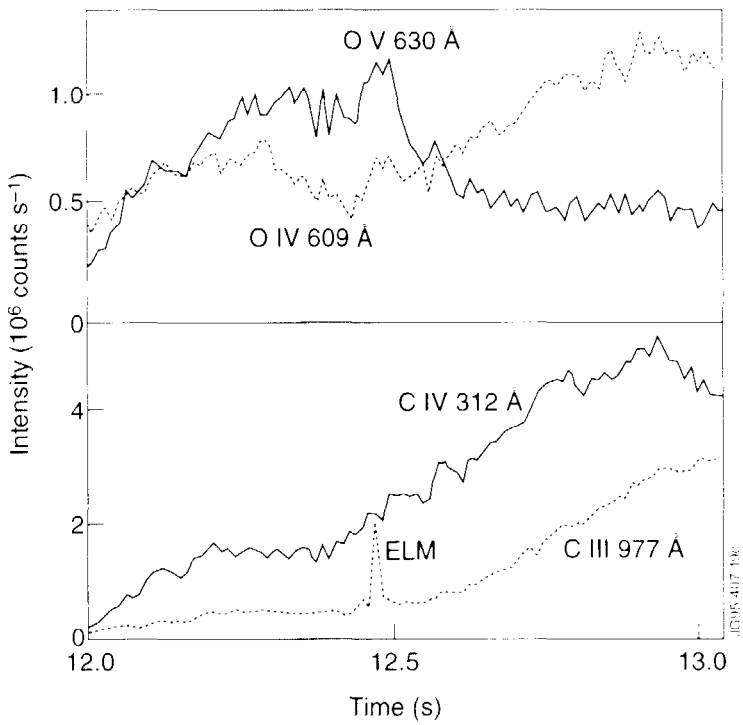

Fig.17b. CIII, CIV, OIV and OV line intensities from the divertor plasma observed with the double SPRED spectrometer for the high performance pulse 32952.